International Journal of Heat and Fluid Flow 31 (2010) 70–82

Contents lists available at ScienceDirect

International Journal of Heat and Fluid Flow

journal homepage: www.elsevier.com/locate/ijhff

# Three-dimensional numerical study of natural convection in an inclined porous cavity with time sinusoidal oscillating boundary conditions

Q.W. Wang *, J. Yang, M. Zeng, G. Wang

*State Key Laboratory of Multiphase Flow in Power Engineering, Xi'an Jiaotong University, Xi'an, Shaanxi 710049, PR China*

ARTICLE INFO

*Article history:*
Received 26 March 2009
Received in revised form 9 September 2009
Accepted 13 November 2009
Available online 24 December 2009

*Keywords:*
Temperature oscillation
Inclined porous cavity
Natural convection
Numerical simulation

ABSTRACT

Three-dimensional unsteady natural convections in an inclined porous cavity with time oscillating boundary conditions are numerically studied in this paper. The Darcy–Forchheimer–Brinkman model is adopted to model the fluid flow in the porous medium and the combination effects of inclination angles ($\alpha_1$, $\alpha_2$) and temperature oscillation frequency ($f$) on the convection characteristics with different Rayleigh numbers ($Ra = 10^6$ and $10^7$) are carefully investigated, especially when the porous cavity is seriously inclined ($80^\circ \leqslant \alpha_1 \leqslant 90^\circ$). It is revealed that, when the porous cavity is moderately inclined ($0^\circ \leqslant \alpha_1 \leqslant 75^\circ, \alpha_2 = 0^\circ$), the natural convections inside are stable and quasi two-dimensional. However, if the cavity is seriously inclined ($75^\circ \leqslant \alpha_1 \leqslant 90^\circ, \alpha_2 = 0^\circ$), the flow patterns inside are much more complicated and the three-dimensional multiple roll-cells with different intercrossing angles are established. It is also found that, when the porous cavity is inclined with three-dimensional method ($\alpha_1 > 0^\circ$, $\alpha_2 > 0^\circ$), the natural convections become quite different and a series of three-dimensional screw type flexural roll-cells appears. Furthermore, it is suggested that, with proper selection of inclination angles and oscillation frequency, the natural convection heat transfer will be significantly improved and the maximal heat fluxes are finally obtained at the optimal combinations of $f = 35\pi$, $\alpha_1 = 50^\circ$, $\alpha_2 = 45^\circ$ when $Ra = 10^6$ and $f = 40\pi$, $\alpha_1 = 45^\circ$, $\alpha_2 = 45^\circ$ when $Ra = 10^7$.



## 1. Introduction

Natural convections in porous media are existed in a wide range of geophysical and engineering applications including geothermal systems, high-performance building insulations, cooling of electronic devices and solar power collectors, etc. Representative studies in this field have been well summarized in the recent books by Pop and Ingham (2001), Nield and Bejan (2006) and Vafai (2005). Some more recent researches can also be found in the references by Oztop (2007), Varol et al. (2008) and Basak et al. (2009). For example, Oztop (2007) has numerically studied the natural convections in a partially cooled and inclined rectangular porous enclosure. The effects of Rayleigh number, inclination angle, aspect ratio and locations of the cooler were carefully investigated. It was found that inclination angle was the dominant parameter on heat transfer and fluid flow as well as aspect ratio. Varol et al. (2008) have performed a theoretical study of natural convections in an inclined trapezoidal enclosure. The effects of Rayleigh number, orientation angle, side wall inclination angle and aspect ratio were considered. It was shown that, the orientation angle was more influential on heat transfer and flow strength than that of the side wall inclination angle. A Benard flow would occur as the orientation angle was around zero, which would also depend on the side wall inclination angle, Rayleigh number and aspect ratio. Furthermore, the phenomena of natural convections in a trapezoidal porous enclosure for linearly heated vertical wall (walls) with various inclination angles were also investigated by Basak et al. (2009). The simulations were performed with different Rayleigh number ($Ra$), Prandtl number ($Pr$), Darcy number ($Da$) and side wall inclination angle. They found that, with different inclination angles and heating methods, the transport phenomena in the porous enclosure were quite different. For example, when the inclination angle equaled 30° and 0° with $Pr = 0.026$ and 0.7, $Da = 10^{-3}$ and $Ra = 10^6$ for linearly heated side walls, the secondary and tertiary circulations multiple circulations would appear at the bottom half of the cavity. While for linearly heated left wall and cold right wall, multiple circulations would occur near the top portion of the cavity. These recent references would be useful for further comprehension of complicated natural convections in the inclined porous enclosures.

Meanwhile, in the past two decades, natural convection in a system with time oscillating boundary conditions has received much attention. Kazmierczak and Chinoda (1992) studied the effect of vertical wall temperature oscillation frequency and amplitude on the heat transfer and fluid flow in a cubic cavity. Xia et al. (1995) researched the effect of wall temperature oscillation

* Corresponding author. Tel./fax: +86 29 82663502.
*E-mail address:* wangqw@mail.xjtu.edu.cn (Q.W. Wang).

0142-727X/$ - see front matter © 2009 Elsevier Inc. All rights reserved.
doi:10.1016/j.ijheatfluidflow.2009.11.005

**Nomenclature**

| | |
|---|---|
| $a$ | effective thermal diffusivity, $m^2\ s^{-1}$ |
| $c_F$ | inertia coefficient |
| $c_p$ | specific heat at constant pressure, $J\ kg^{-1}\ K^{-1}$ |
| $Da$ | Darcy number (Eq. (4)) |
| $f$ | dimensionless oscillating frequency |
| $g$ | gravitational acceleration, $m\ s^{-2}$ |
| $H$ | cavity height (Fig. 2), m |
| $k$ | thermal conductivity, $W\ m^{-1}\ K^{-1}$ |
| $K$ | permeability, $m^2$ |
| $L$ | representative cavity length, m |
| $Nu$ | Nusselt number (Eqs. (8) and (9)) |
| $n$ | number of time-period |
| $p$ | pressure, Pa |
| $P$ | dimensionless pressure |
| $Pr$ | Prandtl number (Eq. (4)) |
| $Ra$ | Rayleigh number (Eq. (4)) |
| $T$ | temperature, K |
| $T_0$ | cold wall temperature, K |
| $T_1$ | temperature oscillation amplitude, K |
| $t$ | time, s |
| $u, v, w$ | velocity in $x, y, z$ directions, $m\ s^{-1}$ |
| $U, V, W$ | dimensionless velocity in $X, Y, Z$ directions |
| $\vec{v}$ | velocity vector, $m\ s^{-1}$ |
| $\vec{V}$ | dimensionless velocity vector, $m\ s^{-1}$ |
| $x, y, z$ | coordinates, m |
| $X, Y, Z$ | dimensionless coordinates |

*Greek symbols*

| | |
|---|---|
| $\alpha$ | inclination angle, ° |
| $\alpha_1$ | inclination angle rotating around $y$ coordinate, ° |
| $\alpha_2$ | inclination angle rotating around $x$ coordinate, ° |
| $\beta$ | thermal expansion coefficient, $K^{-1}$ |
| $\varepsilon$ | porosity |
| $\theta$ | dimensionless temperature |
| $\nu$ | kinetic viscosity, $m^2\ s^{-1}$ |
| $\rho$ | density, $kg\ m^{-3}$ |
| $\rho_0$ | density at $T_0$, $kg\ m^{-3}$ |
| $\sigma$ | specific heat ratio (Eq. (4)) |
| $\tau$ | dimensionless time |
| $\omega$ | oscillating frequency, $s^{-1}$ |

*Subscripts*

| | |
|---|---|
| f | fluid phase |
| Lav | absolute time-averaged value on left side wall |
| m | effective value |
| p | time-period |
| R | average value on right side wall |
| Rav | time-averaged value on right side wall |
| s | solid phase |

variation on the natural convection stability in a cubic enclosure with fixed oscillation frequency. Kwak and Hyun (1996) and Kwak et al. (1998) investigated the resonance effect of the convective heat transfer in a cavity. Soong et al. (2001) analyzed the effects of bottom-wall temperature modulation on the threshold of thermal instability and the oscillatory cellular convection in a rectangular enclosure. Wang et al. (2008) reported the uni-directional heat flux phenomena in a horizontal fluid layer with sinusoidal wall temperature boundary conditions. Similar studies were also performed by Reeve et al. (2004) and Nithyadevi et al. (2006). All these studies indicate that the natural convection heat transfer in a system with time oscillating boundary conditions can be significantly augmented. Similar natural convection heat transfer augmentation technique with time oscillating boundary conditions can also be applied in porous media systems, such as solidification in cast process, cooling of electronic devices and post-accident cooling of nuclear reactors (Rudraiah and Malashetty, 1990). However, the researches on this subject are relatively scarce. Rudraiah and Malashetty (1990) studied the stability and onset of convection in a fluid saturated porous medium layer under periodic vertical temperature gradient. Antohe and Lage (1994) investigated the convection induced by a fixed-amplitude, time-periodic, horizontal heat flux imposed on a saturated porous medium enclosure.

It is worth noting that, Kalabin et al. (2005) reported the time-averaged Nusselt number was not zero for an inclined cubic cavity with a sinusoidal wall temperature on the one side wall and a constant average temperature on the opposing side wall. The system had no temperature difference between the opposing two side walls in a time-average sense and the inclination angle was varying from 0° to 89°. The maximal heat flux was obtained at an inclined angle of 54° and dimensionless frequency of $20\pi$. Their findings could be useful for enhancing and controlling the natural convections in a clear fluid system. Similar phenomena could also be expected to occur in porous media systems. Enlightened by Kalabin et al. (2005), Wang et al. (2008a,b) recently studied the natural convection in inclined porous cavities with one side wall (upward facing) of oscillating temperature and the opposing side wall (downward facing) at constant average temperature. Numerical results were obtained for the values of the inclined angle $0^\circ \leqslant \alpha \leqslant 80^\circ$ and various values of the dimensionless oscillating frequency. They found that, the time-averaged heat flux was always transferred from the upward-facing wall to downward-facing wall for porous cavity. They also obtained the maximal heat flux at an inclined angle of 42.2° and dimensionless frequency of $46.7\pi$. Their findings could be of great significance for enhancing and optimizing the natural convection heat transfer in porous media systems. However, in the above mentioned researches of Kalabin et al. (2005) and Wang et al. (2008a,b), the natural convections in the inclined cavities were modeled with two-dimensional methods and the cavity inclination angles are of $0^\circ \leqslant \alpha \leqslant 89^\circ$ and $0^\circ \leqslant \alpha \leqslant 80^\circ$ respectively. According to the earlier numerical and experimental studies of Ozoe et al. (1974, 1979), if the cavity was seriously inclined ($80^\circ \leqslant \alpha \leqslant 90^\circ$), complex flow pattern with three-dimensional multiple roll-cells would appear in the cavity. Therefore, when the cavity inclination angle is relatively large ($\alpha \geqslant 80^\circ$), the two-dimensional model would be questionable and it is necessary to model the unsteady natural convection inside with three-dimensional method. Furthermore, in all previous studies, the inclined cavity was only rotated around single axis (parallel to the hot and cold surfaces), and the effects of other inclination angles are still unknown, which would also be interesting and important for applications. With these motivations, in the present study, we further study the natural convections in an inclined porous cavity with three-dimensional method, where the boundary conditions are similar to those of Wang et al. (2008a). Our objective is to investigate the three-dimensional natural convection characteristics with the combination effects of inclination angles and temperature oscillation frequency, especially when the porous cavity is seriously inclined, and find out the maximal heat fluxes at optimal combinations of these effects. According to the authors' knowledge, almost no such attentions have been paid to this subject before and the findings would be useful for further understanding and optimizing the natural convection heat transfer in three-dimensional porous media systems.

## 2. Mathematical formulation

As shown in Fig. 1a, a three-dimensional cubic cavity with dimensions of $L \times L \times L$ is filled with porous medium and fluid, where the fluid is a Newtonian incompressible fluid ($Pr$ = 1.0) and the porous medium is homogeneous and isotropic. The temperature on the right side wall ($x = L$) is kept at constant $T_0$ and it is sinusoidal oscillating with time at a mean temperature $T_0$ on the opposing side wall ($x = 0$). The top, bottom and two other side walls are all kept adiabatic. In the present study, the cavity is inclined around both $x$ and $y$ axes with $\alpha_1$ and $\alpha_2$ respectively to account for the three-dimensional inclination effects. Firstly, $\alpha_2$ is fixed at 0° and the cavity is inclined around $y$-axis with $\alpha_1$ from 0° to 90° (see Fig. 1b). Then, $\alpha_1$ is fixed at a constant degree and the cavity is inclined around $x$-axis with $\alpha_2$ from 0° to 90° (see Fig. 1c).

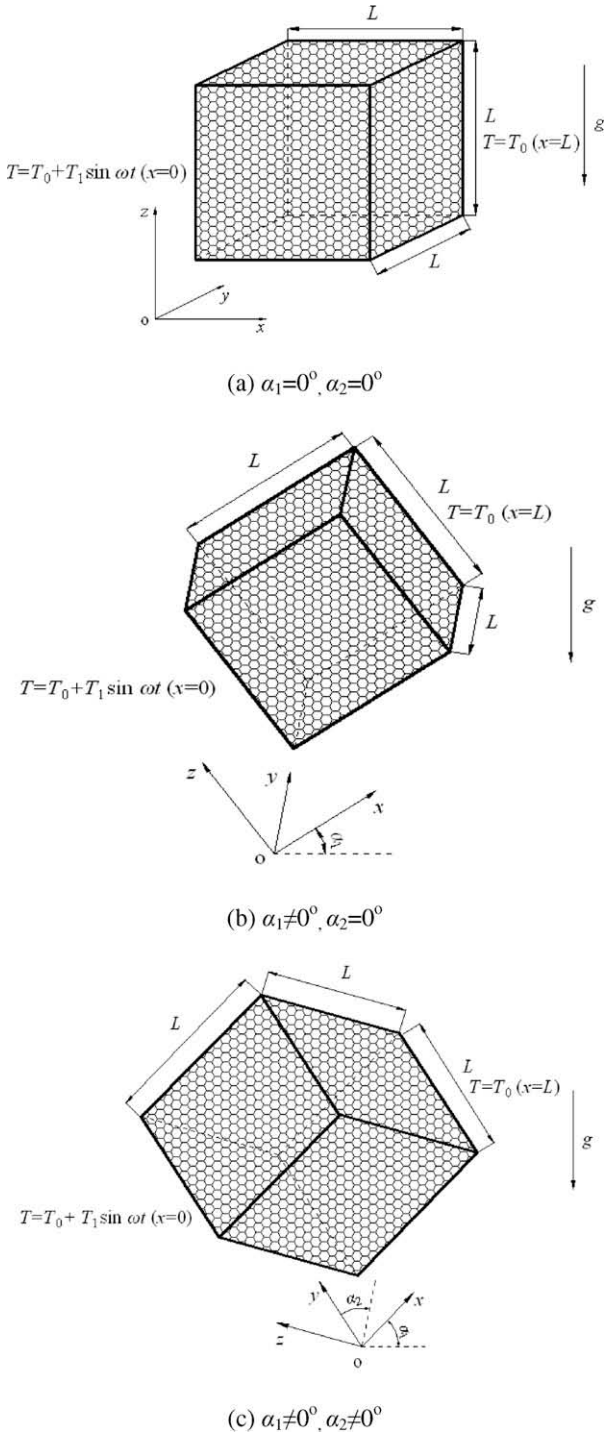


**Fig. 1.** Physical models.

In the present study, the natural convection in the cubic cavity is considered to be three-dimensional, laminar, incompressible and unsteady. The porous medium is assumed to be in local thermal equilibrium with the fluid. The thermophysical properties of the fluid and the porous material are taken to be constant except for the density variation in the buoyancy force, which is treated by using the Boussinesq approximation. The Darcy–Forchheimer–Brinkman model (Nield and Bejan, 2006) is adopted to simulate the flow in porous medium, where both the inertia and viscosity effects are considered. The conservation equations for mass, momentum and energy are as follows:

Continuity:

$$\nabla \cdot \vec{v} = 0 \tag{1}$$

Momentum:

$$\begin{cases} \dfrac{1}{\varepsilon}\dfrac{\partial u}{\partial t} + \dfrac{1}{\varepsilon^2}(\vec{v}\cdot\nabla u) = -\dfrac{1}{\rho_f}\dfrac{\partial p}{\partial x} + \nu_m\nabla^2 u - \dfrac{\nu_f}{K}u \\ \qquad\qquad - \dfrac{c_F}{\sqrt{K}}|\vec{v}|u + \beta(T-T_0)g\sin\alpha_1 \\ \dfrac{1}{\varepsilon}\dfrac{\partial v}{\partial t} + \dfrac{1}{\varepsilon^2}(\vec{v}\cdot\nabla v) = -\dfrac{1}{\rho_f}\dfrac{\partial p}{\partial y} + \nu_m\nabla^2 v - \dfrac{\nu_f}{K}v \\ \qquad\qquad - \dfrac{c_F}{\sqrt{K}}|\vec{v}|v + \beta(T-T_0)g\cos\alpha_1\sin\alpha_2 \\ \dfrac{1}{\varepsilon}\dfrac{\partial w}{\partial t} + \dfrac{1}{\varepsilon^2}(\vec{v}\cdot\nabla w) = -\dfrac{1}{\rho_f}\dfrac{\partial p}{\partial z} + \nu_m\nabla^2 w - \dfrac{\nu_f}{K}w \\ \qquad\qquad - \dfrac{c_F}{\sqrt{K}}|\vec{v}|w + \beta(T-T_0)g\cos\alpha_1\cos\alpha_2 \end{cases} \tag{2}$$

Energy:

$$(\rho C_p)_m\frac{\partial T}{\partial t} + (\rho C_p)_f\cdot\vec{v}\cdot\nabla T = k_m\nabla^2 T \tag{3}$$

where $\beta$ is the fluid thermal expansion coefficient. $\vec{v}$ is the velocity vector. $\varepsilon$ and $K$ are the porosity and permeability of the porous medium, respectively. $c_F$ is the inertia coefficient of the porous medium, $c_F = 1.75/(\sqrt{150}\cdot\varepsilon^{1.5})$ (Ergun, 1952). $k_m$ is the effective thermal conductivity of porous medium, $k_m = (1-\varepsilon)k_s + \varepsilon k_f$, where $k_s$ and $k_f$ are the thermal conductivities of the solid framework and fluid, respectively. $\nu_m$ is the effective kinetic viscosity of porous medium. The value of $\nu_f$ is used as an approximate value of $\nu_m$ and this

**Table 1**
Absolute time-averaged Nusselt numbers on the left side wall with different grids within the 3rd to 5th time-periods ($Ra = 10^6$, $Da = 10^{-3}$, $Pr$ = 1.0, $\varepsilon$ = 0.6, $\sigma$ = 1.0, $f = 20\pi$, $\tau_p$ = 0.1, $\alpha_1$ = 0° and $\alpha_2$ = 0°).

| Grids | 30 × 30 × 30 | 40 × 40 × 40 | 50 × 50 × 50 |
|---|---|---|---|
| $Nu_{Lav}$ (3rd time-period) | 8.871 | 8.793 | 8.766 |
| $Nu_{Lav}$ (4th time-period) | 8.875 | 8.794 | 8.769 |
| $Nu_{Lav}$ (5th time-period) | 8.875 | 8.794 | 8.770 |

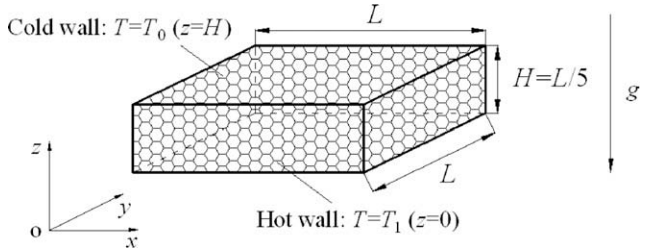


**Fig. 2.** Physical model reported by Kladias and Prasad (1991).

**Table 2**
Comparisons of the average Nusselt number between present computations and experiments reported by Kladias and Prasad (1991).

| Cases | $\varepsilon$ | $Da$ | $Pr$ | $Ra$ | $Nu$ | |
|---|---|---|---|---|---|---|
| | | | | | Present | Kladias and Prasad (1991) |
| 1 | 0.375 | $1.16 \times 10^{-6}$ | 4.0 | $4.05 \times 10^{8}$ | 6.05 | 6.41 |
| 2 | 0.396 | $5.84 \times 10^{-6}$ | 4.0 | $1.10 \times 10^{8}$ | 6.76 | 6.28 |
| 3 | 0.453 | $7.78 \times 10^{-5}$ | 4.0 | $0.80 \times 10^{7}$ | 5.99 | 6.19 |
| 4 | 0.453 | $7.78 \times 10^{-5}$ | 4.0 | $2.28 \times 10^{7}$ | 9.84 | 10.35 |

approximation provides good agreement with experiment data obtained by Lundgren (1972).

The initial and boundary conditions are as follows:

$$\begin{cases} t = 0, & u = v = w = 0, & T = T_0 \\ x = 0, & u = v = w = 0, & T = T_0 + T_1 \sin \omega t \\ x = L, & u = v = w = 0, & T = T_0 \\ y = 0, L & u = v = w = 0, & \partial T/\partial y = 0 \\ z = 0, L & u = v = w = 0, & \partial T/\partial z = 0 \end{cases}$$

where $\omega$ is the temperature oscillation frequency.

It is convenient to cast the above governing equations in terms of dimensionless variables as follows:

$$\begin{cases} \tau = t a_m/L^2; \quad X = x/L; \quad Y = y/L; \quad Z = z/L; \\ U = uL/a_m; \quad V = vL/a_m; \quad W = wL/a_m; \quad P = pL^2/(\rho_0 a_m^2); \\ \theta = (T - T_0)/(T_1 - T_0); \quad \sigma = (\rho c_p)_m/(\rho c_p)_f; \quad Pr = \nu_f/a_m; \\ Da = K/L^2; \quad Ra = g\beta(T_1 - T_0)L^3/(\nu_f a_m) \end{cases} \tag{4}$$

where $\sigma$ is the specific heat ratio. $Pr$ and $Da$ are the Prandtl number and Darcy number, respectively. $a_m$ is the effective thermal diffusivity of the porous medium, $a_m = k_m/(\rho c_p)_f$.

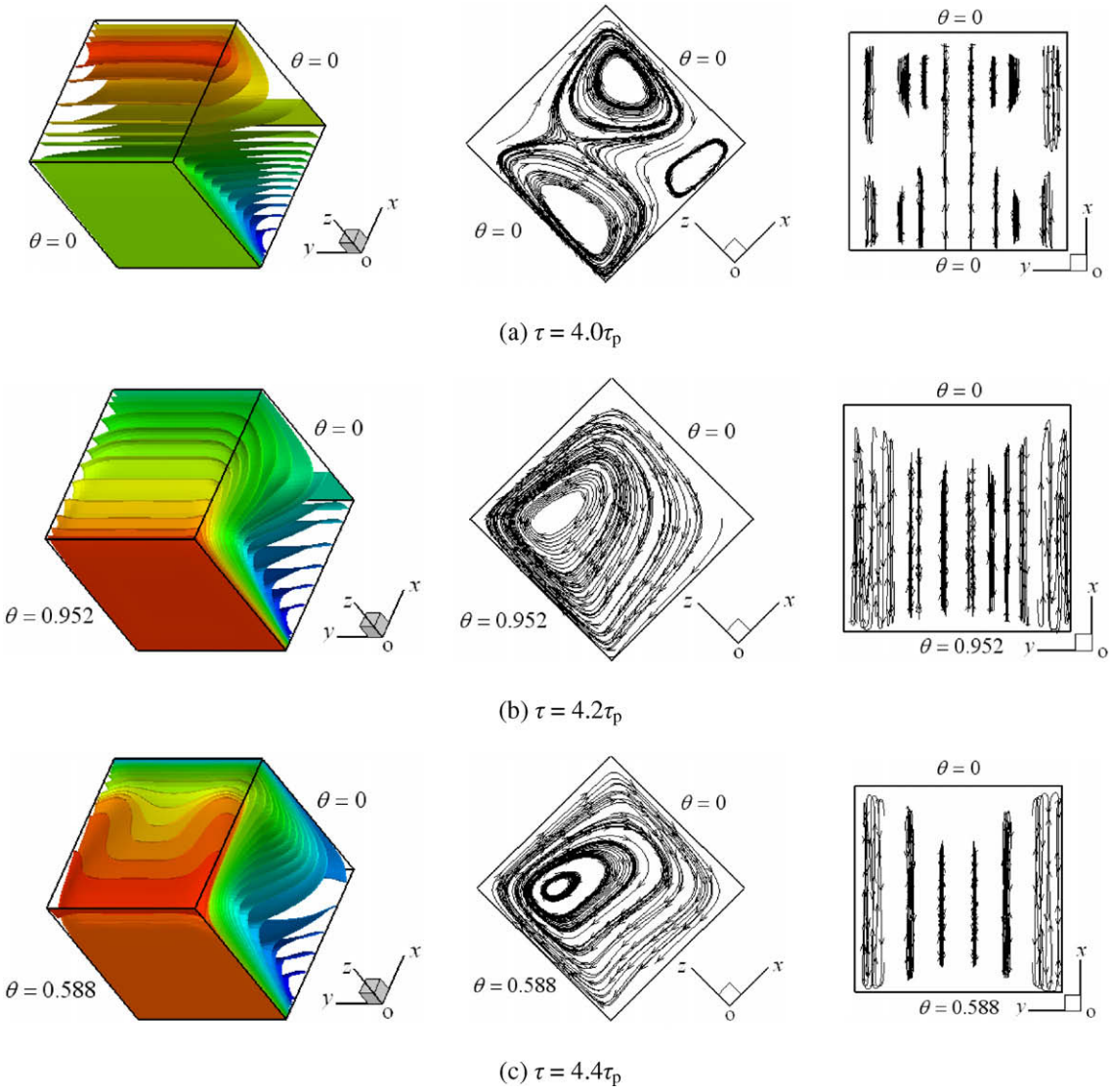


**Fig. 3.** Transient temperature (left column) and streamline (middle and right columns) distributions within the 5th time-period ($Ra = 10^6$, $Da = 10^{-3}$, $Pr = 1.0$, $\varepsilon = 0.6$, $\sigma = 1.0$, $f = 20\pi$, $\tau_p = 0.1$, $\alpha_1 = 45°$ and $\alpha_2 = 0°$).

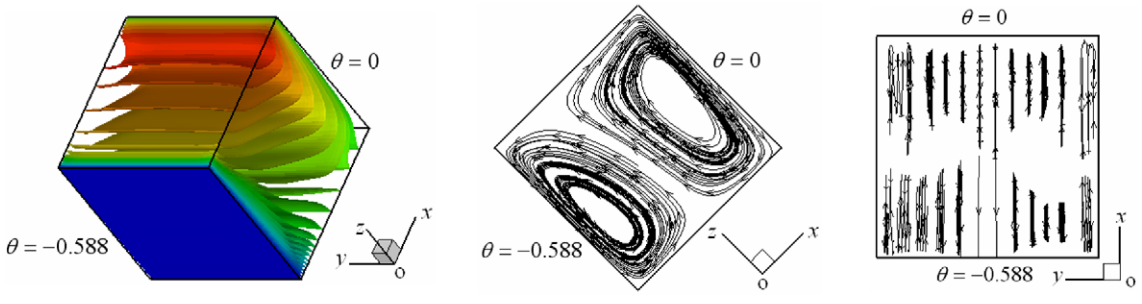


(d) $\tau = 4.6\tau_p$

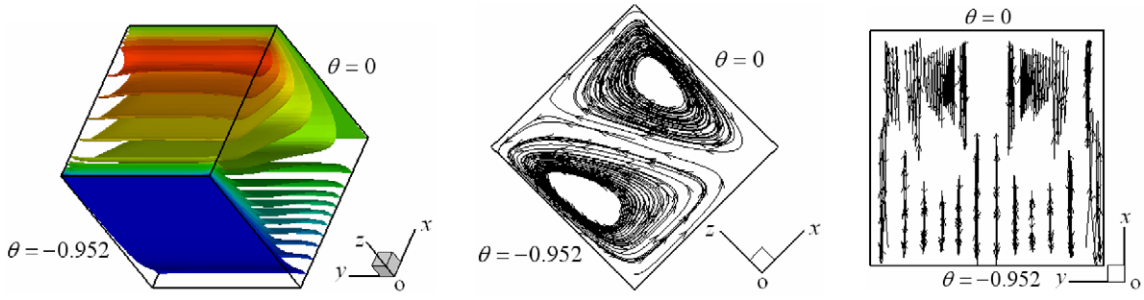


(e) $\tau = 4.8\tau_p$

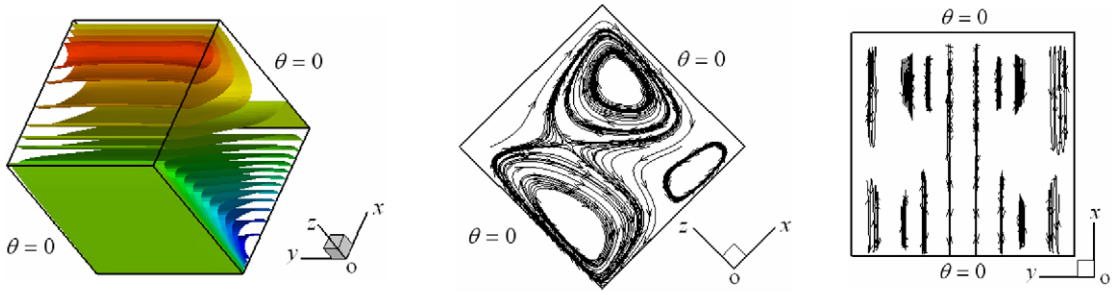


(f) $\tau = 5.0\tau_p$

**Fig. 3**. (*continued*).

Substitute these dimensionless variables into Eqs. (1)–(3), the corresponding dimensionless conservation equations for mass, momentum and energy can be obtained as follows:

Continuity:

$$\nabla \cdot \vec{V} = 0 \tag{5}$$

Momentum:

$$\begin{cases} \dfrac{1}{\varepsilon}\dfrac{\partial U}{\partial \tau} + \dfrac{1}{\varepsilon^2}(\vec{V}\cdot\nabla U) = -\dfrac{\partial P}{\partial X} + Pr\nabla^2 U - \dfrac{Pr}{Da}U \\ \qquad\qquad - \dfrac{c_F}{\sqrt{Da}}|\vec{V}|U + RaPr\theta\sin\alpha_1 \\ \dfrac{1}{\varepsilon}\dfrac{\partial V}{\partial \tau} + \dfrac{1}{\varepsilon^2}(\vec{V}\cdot\nabla V) = -\dfrac{\partial P}{\partial Y} + Pr\nabla^2 V - \dfrac{Pr}{Da}V \\ \qquad\qquad - \dfrac{c_F}{\sqrt{Da}}|\vec{V}|V + RaPr\theta\cos\alpha_1\sin\alpha_2 \\ \dfrac{1}{\varepsilon}\dfrac{\partial W}{\partial \tau} + \dfrac{1}{\varepsilon^2}(\vec{V}\cdot\nabla W) = -\dfrac{\partial P}{\partial Z} + Pr\nabla^2 W - \dfrac{Pr}{Da}W \\ \qquad\qquad - \dfrac{c_F}{\sqrt{Da}}|\vec{V}|W + RaPr\theta\cos\alpha_1\cos\alpha_2 \end{cases} \tag{6}$$

Energy:

$$\sigma\frac{\partial \theta}{\partial \tau} + \vec{V}\cdot\nabla\theta = \nabla^2\theta \tag{7}$$

The dimensionless initial and boundary conditions are as follows:

$$\begin{cases} \tau = 0 & U = V = W = 0, \quad \theta = 0, \quad P = 0 \\ X = 0 & U = V = W = 0, \quad \theta = \sin f\tau \\ X = 1 & U = V = W = 0, \quad \theta = 0 \\ Y = 0,1 & U = V = W = 0, \quad \partial\theta/\partial Y = 0 \\ Z = 0,1 & U = V = W = 0, \quad \partial\theta/\partial Z = 0 \end{cases}$$

where $f$ is the dimensionless temperature oscillation frequency, $f = \omega L^2/a_m$.

The absolute time-averaged Nusselt number on the left side wall ($X = 0$) are defined as follow:

$$Nu_{Lav} = \frac{1}{\tau_p}\int_{(n-1)\tau_p}^{n\tau_p}\int_0^1\int_0^1 \left|\frac{\partial\theta}{\partial X}\right|_{X=0} dYdZd\tau \tag{8}$$

The average Nusselt number and the time-averaged Nusselt number on the right side wall ($X = 1$) are defined as follows:

$$Nu_R = -\int_0^1 \int_0^1 \left.\frac{\partial\theta}{\partial X}\right|_{X=1} dYdZ,$$
$$Nu_{Rav} = \frac{1}{\tau_p}\int_{(n-1)\tau_p}^{n\tau_p} \int_0^1 \int_0^1 \left.\frac{\partial\theta}{\partial X}\right|_{X=1} dYdZd\tau \quad (9)$$

where $\tau_p$ is the dimensionless time-period with the definition of $\tau_p = 2\pi/f$ and $n$ is the number of time-period.

## 3. Numerical method and model validation

The dimensionless governing equations (Eqs. (5)–(7)) in the present study are solved with the control volume procedure outlined by Patankar (1980). The SIMPLE algorithm is employed to couple the velocities and pressure. A fully implicit scheme is applied for discretizing the time derivatives. The convective terms are discretized by using the QUICK scheme and a second-order central difference scheme is used for the diffusion terms. The resulting algebraic equations are solved by the tri-diagonal matrix algorithm (TDMA). For convergence criteria, the relative variations of the temperature and velocity between two successive iterations are demanded to be smaller than the previously specified accuracy levels of $10^{-5}$.

Before proceeding further, the grids independence tests are performed at first. As shown in Fig. 1a, the cavity is not inclined and the values of $\alpha_1$, $\alpha_2$ are kept at 0°. The temperature oscillation frequency ($f$) is $20\pi$ and other parameters are kept at constant with $Ra = 10^6$, $Da = 10^{-3}$, $Pr = 1.0$, $\varepsilon = 0.6$, $\sigma = 1.0$. Three sets of uniform and un-staggered grids are used for the tests: $30 \times 30 \times 30$, $40 \times 40 \times 40$ and $50 \times 50 \times 50$. The computational results are presented in Table 1. It is shown that, the differences of the absolute time-averaged Nusselt numbers on the left side wall ($Nu_{Lav}$, $X = 0$) within the 3rd to 5th time-periods are insignificant between $40 \times 40 \times 40$ and $50 \times 50 \times 50$ grids. Therefore, the grid of

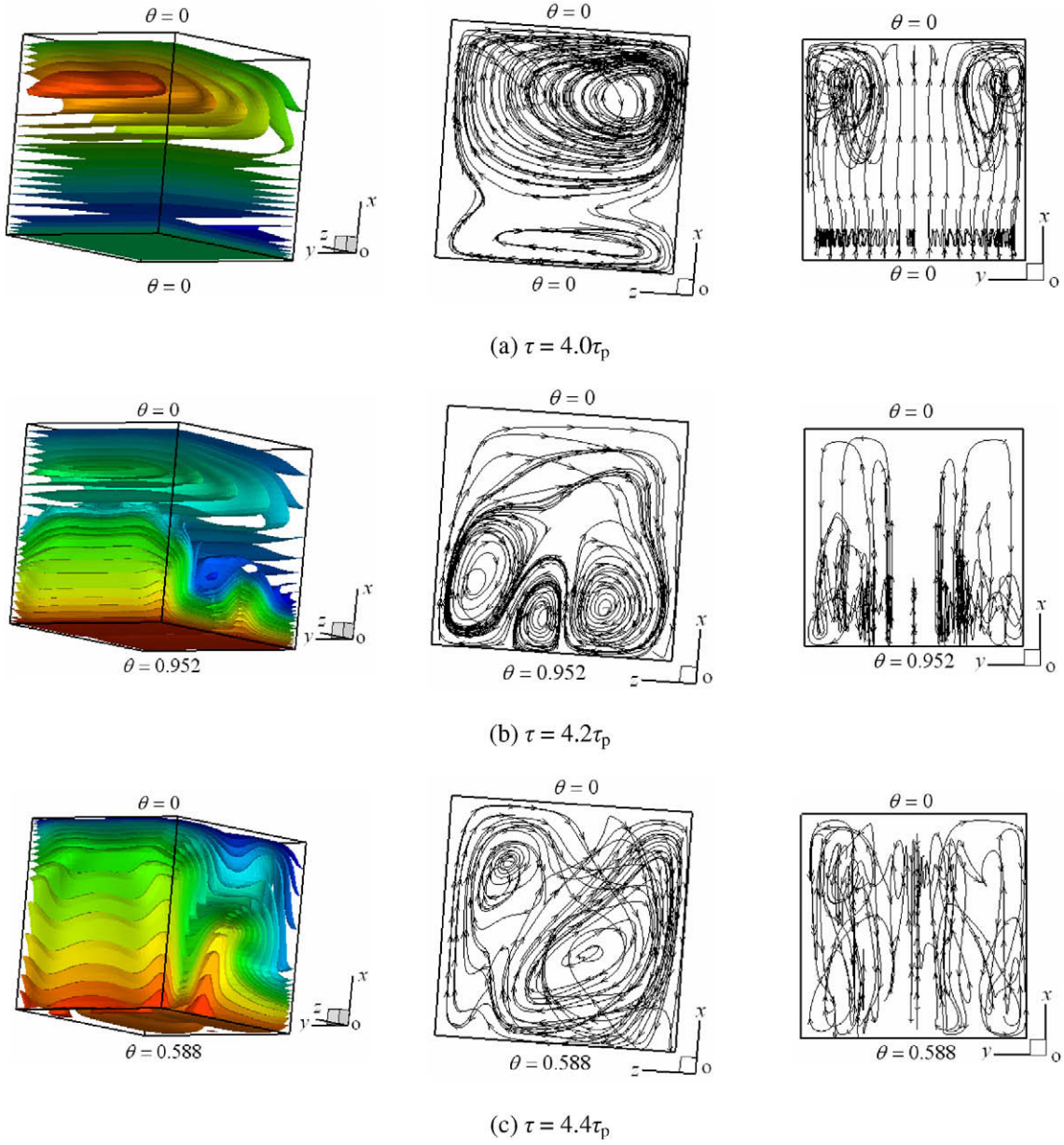


**Fig. 4.** Transient temperature (left column) and streamline (middle and right columns) distributions within the 5th time-period ($Ra = 10^6$, $Da = 10^{-3}$, $Pr = 1.0$, $\varepsilon = 0.6$, $\sigma = 1.0$, $f = 20\pi$, $\tau_p = 0.1$, $\alpha_1 = 86°$ and $\alpha_2 = 0°$).

$40 \times 40 \times 40$ is finally employed for the following studies. Furthermore, it can be found that, with the same grid, the predicted values of $Nu_{Lav}$ within the 4th and 5th time-periods are very close to each other. Therefore, for the following computations, five time-periods are needed for each case.

Furthermore, in order to validate the reliability and accuracy of the present computational model and self-developed code, quantitative comparisons are carried out with the experimental results reported by Kladias and Prasad (1991). The experimental problem is shown in Fig. 2, where a three dimensional rectangular cavity with dimensions of $L \times L \times H$ is filled with porous media and fluid ($Pr = 4.0$). The cavity is heated from bottom ($T = T_1$) and cooled on top ($T = T_0$). All other walls are kept adiabatic. The predicted and experimental average Nusselt numbers are compared in Table 2. The average deviation of Nusselt numbers is 5.4%. This indicates that, the present computational model and self-developed code are reliable and capable of modeling the natural convection phenomena in three-dimensional porous systems.

## 4. Results and discussion

### 4.1. Effect of inclination angle $\alpha_1$

As shown in Fig. 1b, the porous cavity is inclined around $y$-axis step by step with the inclination angle $\alpha_1$ from 0° to 90°, and the inclination angle $\alpha_2$ (rotating around $x$-axis) is fixed at 0°. In this case, the effect of $\alpha_1$ is carefully investigated with $Ra = 10^6$ and $10^7$, especially when the cavity is seriously inclined ($80° \leqslant \alpha_1 \leqslant 90°$). The computations are performed with other parameters kept constant: $Da = 10^{-3}$, $Pr = 1.0$, $\varepsilon = 0.6$, $\sigma = 1.0$ and $f = 20\pi$.

Firstly, the transient temperature and streamline distributions in the porous cavity with moderate inclination angles ($\alpha_1 = 45°$, $\alpha_2 = 0°$) and $Ra = 10^6$ are presented in Fig. 3. It is clearly shown that, the buoyancies are generated from the hot walls and the temperature fields at each moment of the time-period are all quite symmetrical. The streamline distributions at each moment of the time-period are stable and regular. At the beginning of the

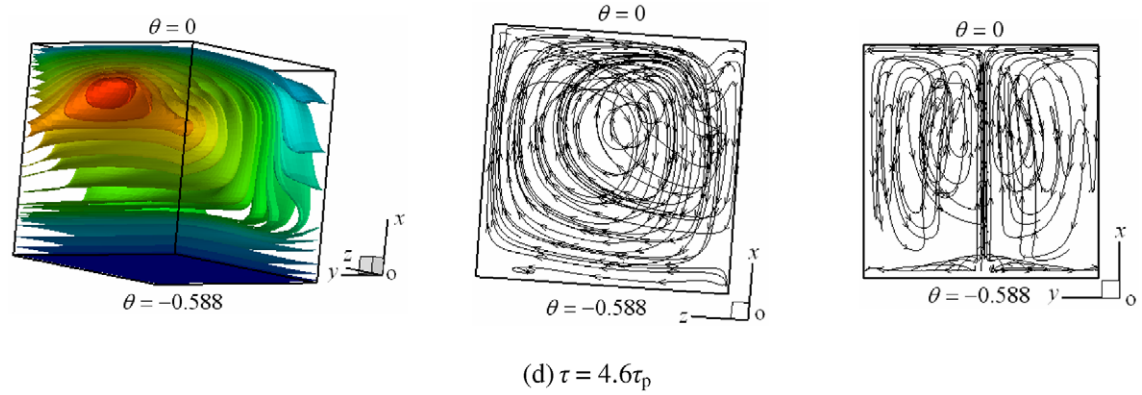


(d) $\tau = 4.6\tau_p$

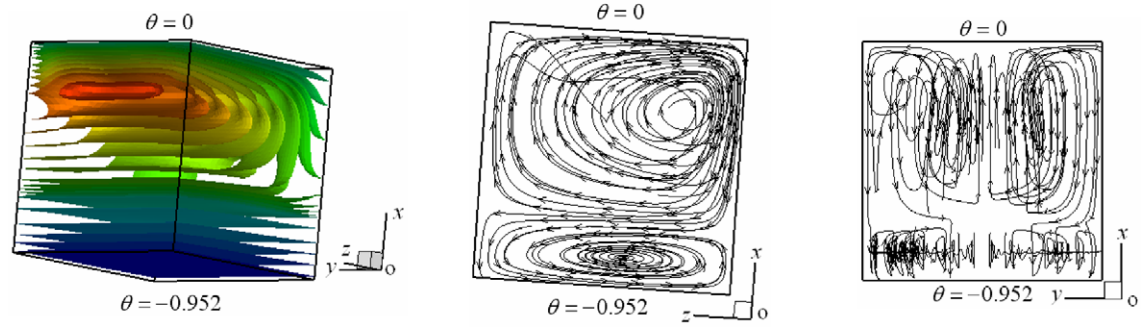


(e) $\tau = 4.8\tau_p$

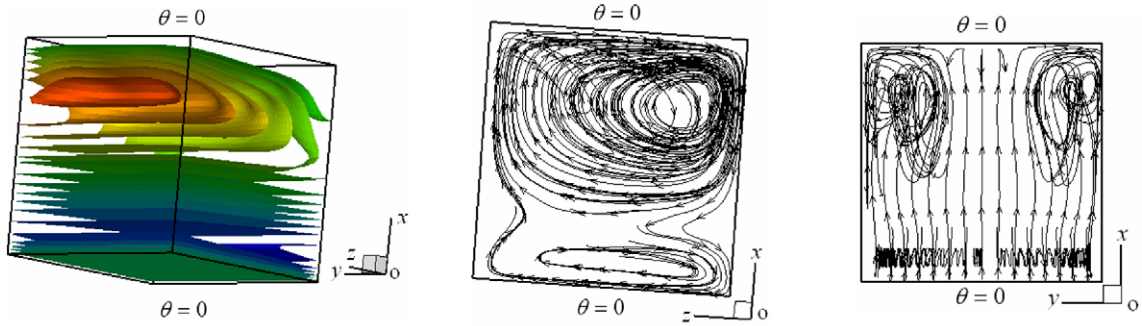


(f) $\tau = 5.0\tau_p$

**Fig. 4**. (*continued*).

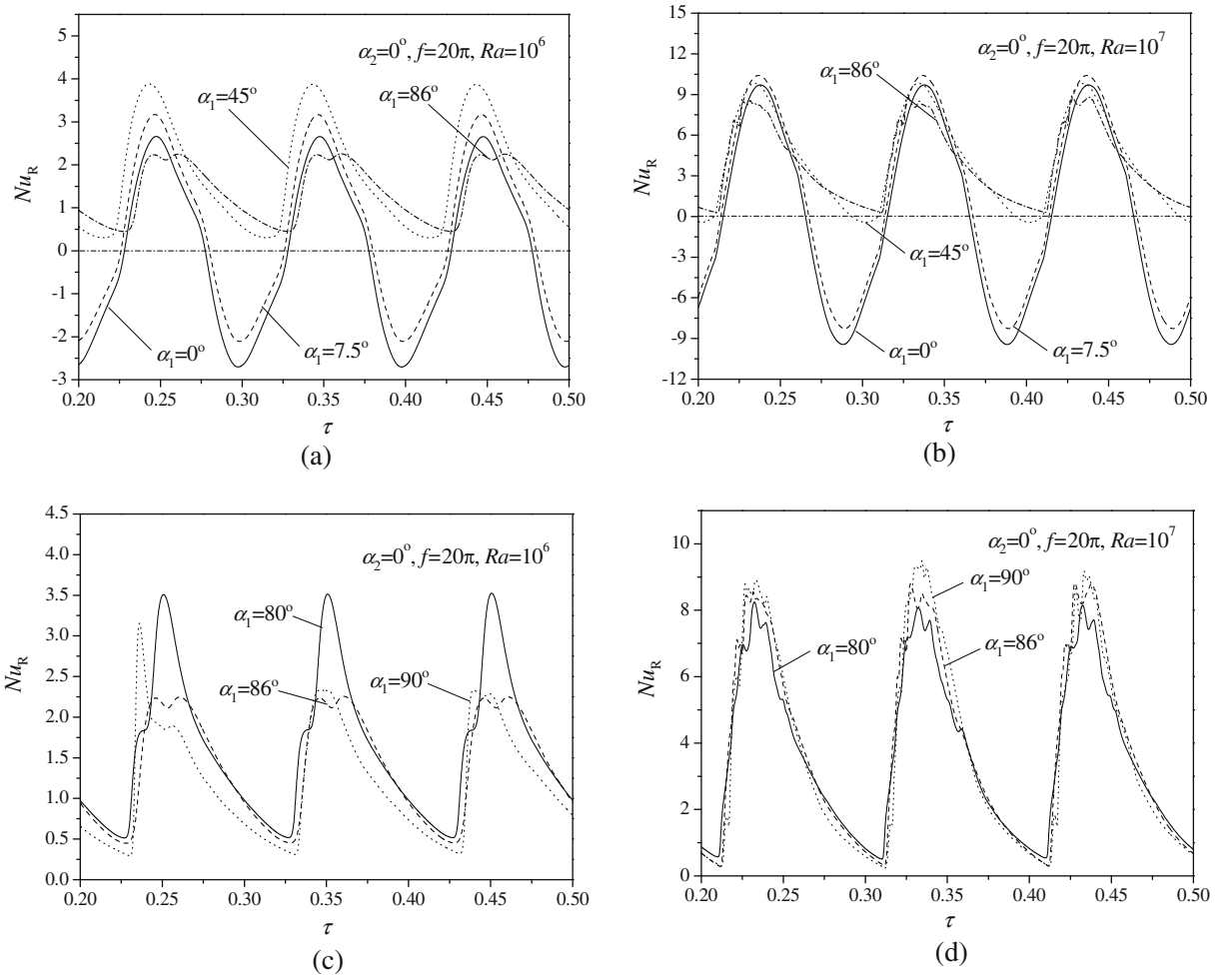


**Fig. 5.** Variations of the average Nusselt number on the right side wall with time for different $\alpha_1$ ($Da = 10^{-3}$, $Pr = 1.0$, $\varepsilon = 0.6$, $\sigma = 1.0$, $f = 20\pi$, $\tau_p = 0.1$ and $\alpha_2 = 0°$).

time-period ($\tau = 4.0\tau_p$, see Fig. 3a), there exist two large clockwise roll-cells in the lower and upper regions of the cavity. Meanwhile, in the right corner of the cavity, there exists a relatively small counterclockwise roll-cell. As time increases, the cavity is mainly occupied with a single large clockwise roll-cell ($\tau = 4.2\tau_p$ and $4.4\tau_p$, see Fig. 3b and c). After then, the cavity is occupied with two large roll-cells rotating in reverse directions ($\tau = 4.6\tau_p$ and $4.8\tau_p$, see Fig. 3d and e), where the upper roll-cell is rotating in clockwise direction and the lower one is rotating in counterclockwise direction. At the end of the time-period ($\tau = 5.0\tau_p$, see Fig. 3f), the streamline distribution returns to the beginning of the time-period ($\tau = 4.0\tau_p$, see Fig. 3a). Furthermore, it is obvious that, all these roll-cells are parallel to each other and their rotating axes are perpendicular to $x$–$z$-surface. These findings indicate that, when the porous cavity is moderately inclined, the flow patterns inside are quasi two-dimensional and the transition phenomena are similar to those of Wang et al. (2008a). However, if the porous cavity is more seriously inclined ($\alpha_1 \geqslant 80°, \alpha_2 = 0°$), the flow patterns inside would be more complex and the transport phenomena should be quite different. The transient temperature and streamline distributions in a seriously inclined porous cavity ($\alpha_1 = 86°$, $\alpha_2 = 0°$) with $Ra = 10^6$ are presented in Fig. 4. Compared with those demonstrated in Fig. 3, it can be found that, in this case ($\alpha_1 = 86°$, $\alpha_2 = 0°$), the temperature fields and flow patterns at each moment of the time-period are much more complicated and the three-dimensional characteristics are very remarkable, especially when the cavity is heated from below ($\tau = 4.2\tau_p$ and $4.4\tau_p$, see Fig. 4b and c). Furthermore, it is obvious that, at each moment of the time-period, the porous cavity is mainly occupied with pairs of multiple roll-cells. These roll-cells are not parallel to each other any more and their rotating axes are intercrossed with different angles. These findings reveal that, when the porous cavity is seriously inclined, the complex flow patterns with three-dimensional

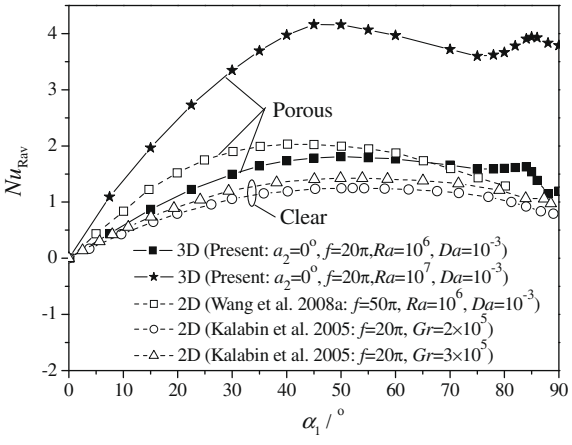


**Fig. 6.** Variations of the time-averaged Nusselt number on the right side wall with $\alpha_1$ ($Da = 10^{-3}$, $Pr = 1.0$, $\varepsilon = 0.6$, $\sigma = 1.0$, $f = 20\pi$, $\tau_p = 0.1$ and $\alpha_2 = 0°$).

multiple roll-cells will be established and the two-dimensional model of Wang et al. (2008a,b) is infeasible any more.

The periodic oscillations of average Nusselt number on the right side wall ($Nu_R$, $X = 1$) with $Ra = 10^6$ and $Ra = 10^7$ are presented in Fig. 5. It is shown that, when $\alpha_1$ equals 0° (see Fig. 5a and b), the Nusselt number $Nu_R$ is oscillating with identical values of positive and negative amplitudes, which indicates the net heat flux from the oscillating temperature wall ($X = 0$) to the constant temperature wall ($X = 1$) is zero. As the inclined angle increases, the Nusselt number becomes larger than zero when it is integrated in time. This suggests that, the heat flux is positive from the oscillating temperature wall ($X = 0$) to the constant temperature wall ($X = 1$) in spite of the net zero temperature difference between these two walls in a time-averaged sense. These findings agree with the two-dimensional results for both the clear (Kalabin et al., 2005) and porous flows (Wang et al., 2008a). Furthermore, it is found that, when the porous cavity is seriously inclined ($\alpha_1 = 80°$, 86° and 90°, see Fig. 5c and d), the oscillations of the Nusselt number become quite different. There exist several extra twists in the curves of $Nu_R$ and the curves are seriously deviated from the sinusoidal law. When the porous cavity is seriously inclined, the flow patterns inside are unstable and three-dimensional multiple roll-cells are established, especially when the cavity is heated from below (see Fig. 4b and c), which would lead to the irregular oscillations for the Nusselt numbers. The variations of the time-averaged Nusselt number on the right side wall ($Nu_{Rav}$, $X = 1$) with $Ra = 10^6$ and $Ra = 10^7$ are presented in Fig. 6. It shows that, when $\alpha_1$ changes from 0° to 75°, the Nusselt number increases first and then decreases smoothly. The maximal heat fluxes are obtained at $\alpha_1 = 50°$ ($\alpha_2 = 0°$) as $Ra$ equals $10^6$ and $\alpha_1 = 45°$ ($\alpha_2 = 0°$) as $Ra$ equals $10^7$, respectively. This is similar to the results of Kalabin et al. (2005) and Wang et al. (2008a). However, when $\alpha_1$ is located in the range of 75°–90°, the variation of the Nusselt number becomes quite different. There exists a local peak in each curve of $Nu_{Rav}$ and the local maximal heat fluxes are obtained at $\alpha_1 = 84°$ when $Ra = 10^6$ and $\alpha_1 = 85°$ when $Ra = 10^7$, respectively. This confirms that, when the porous cavity is moderately inclined, the natural convections inside would be stable, regular and quasi two-dimen-

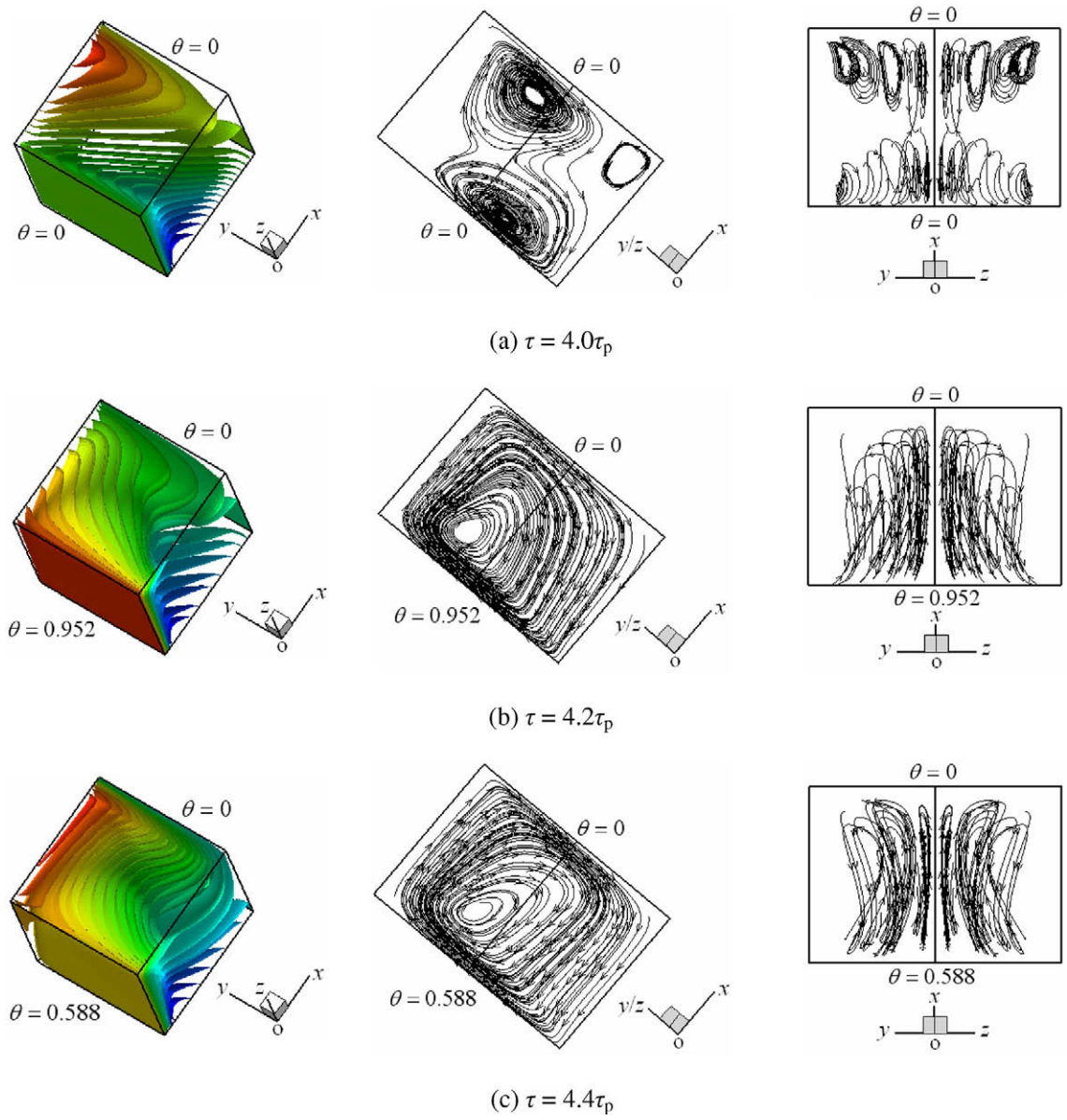


**Fig. 7.** Transient temperature (left column) and streamline (middle and right columns) distributions within the 5th time-period ($Ra = 10^6$, $Da = 10^{-3}$, $Pr = 1.0$, $\varepsilon = 0.6$, $\sigma = 1.0$, $f = 20\pi$, $\tau_p = 0.1$, $\alpha_1 = 50°$ and $\alpha_2 = 45°$).

sional. However, when the porous cavity is seriously inclined, the natural convections inside are unstable and three-dimensional, which finally leads to complicated heat transfer performances.

### 4.2. Effect of three-dimensional inclinations

As shown in Fig. 1c, the porous cavity is inclined around both $x$ and $y$ axes to account for the three-dimensional inclination effects and find out the optimal inclination angles. According to above analysis, it is learned that, when the porous cavity is only rotated around $y$-axis, the maximal heat fluxes are obtained at $\alpha_1 = 50°$ ($\alpha_2 = 0°$) when $Ra = 10^6$ and $\alpha_1 = 45°$ ($\alpha_2 = 0°$) when $Ra = 10^7$, respectively. Therefore, in this case, the porous cavity is firstly rotated around $y$-axis with $\alpha_1 = 50°$ as $Ra$ equals $10^6$ and $\alpha_1 = 45°$ as $Ra$ equals $10^7$, respectively, and then it is rotated around $x$-axis step by step with $\alpha_2$ from 0° to 90°. The computations are performed with other parameters kept constant: $Da = 10^{-3}$, $Pr = 1.0$, $\varepsilon = 0.6$, $\sigma = 1.0$ and $f = 20\pi$.

The transient temperature and streamline distributions in the porous cavity with representative inclination angles ($\alpha_1 = 50°$, $\alpha_2 = 45°$) with $Ra = 10^6$ are presented in Fig. 7. It is shown that, the temperature fields and flow patterns at each moment of the time-period are symmetrical and stable. At the beginning of the time-period ($\tau = 4.0\tau_p$, see Fig. 7a), there exist three roll-cells in the porous cavity, two large clockwise roll-cells are in the upper and lower regions and a small counterclockwise roll-cell is in the corner. As time increases, the roll-cells are merged to be a larger single clockwise roll-cell ($\tau = 4.2\tau_p$ and $4.4\tau_p$, see Fig. 7b and c). After then, the cavity is occupied with two large roll-cells ($\tau = 4.6\tau_p$ and $4.8\tau_p$, see Fig. 7d and e), where the upper roll-cell is rotating in clockwise direction and the lower one is rotating reversely. At the end of the time-period ($\tau = 5.0\tau_p$, see Fig. 7f), the flow pattern is back to the beginning of the time-period ($\tau = 4.0\tau_p$, see Fig. 7a). These transitions are similar to those demonstrated in Fig. 3 ($\alpha_1 = 45°$, $\alpha_2 = 0°$). However, in this case ($\alpha_1 = 50°$, $\alpha_2 = 45°$), the temperature fields and flow patterns are more complex and the three-dimensional characteristics are quite remarkable. At each moment of the time-period, the porous cavity is mainly occupied with pairs of symmetrical screw type flexural roll-cells and their rotating axes are intercrossed with each other.

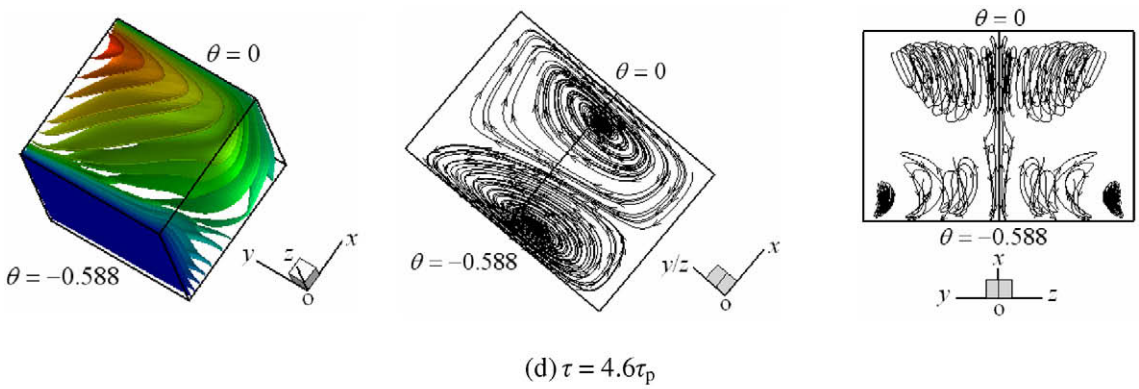


(d) $\tau = 4.6\tau_p$

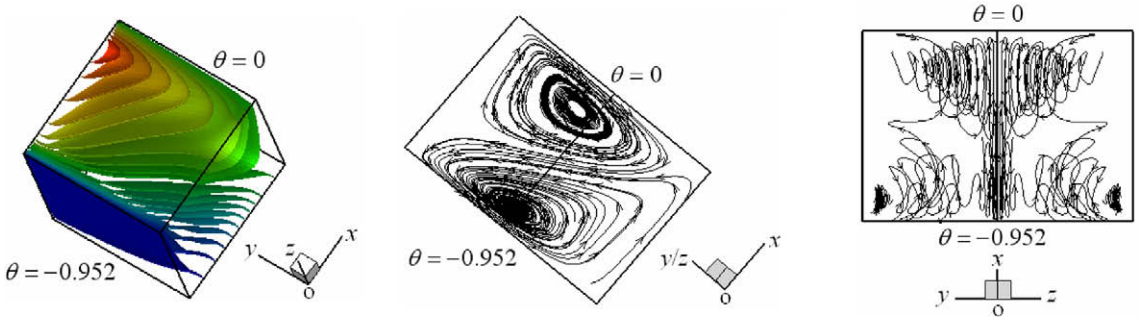


(e) $\tau = 4.8\tau_p$

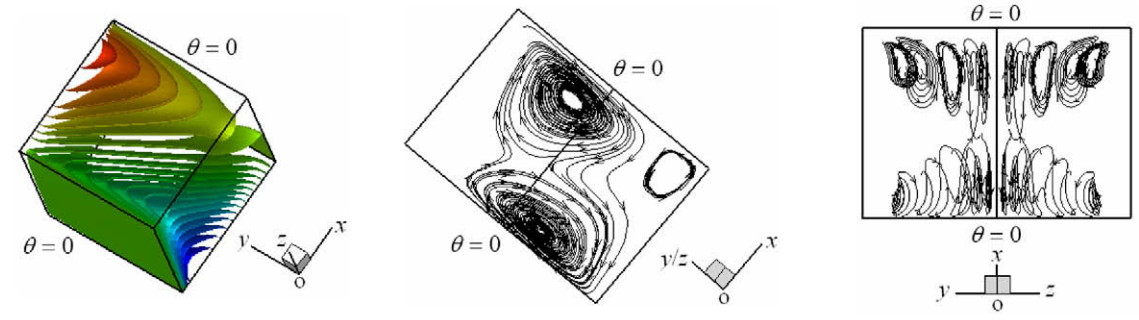


(f) $\tau = 5.0\tau_p$

**Fig. 7**. (*continued*).

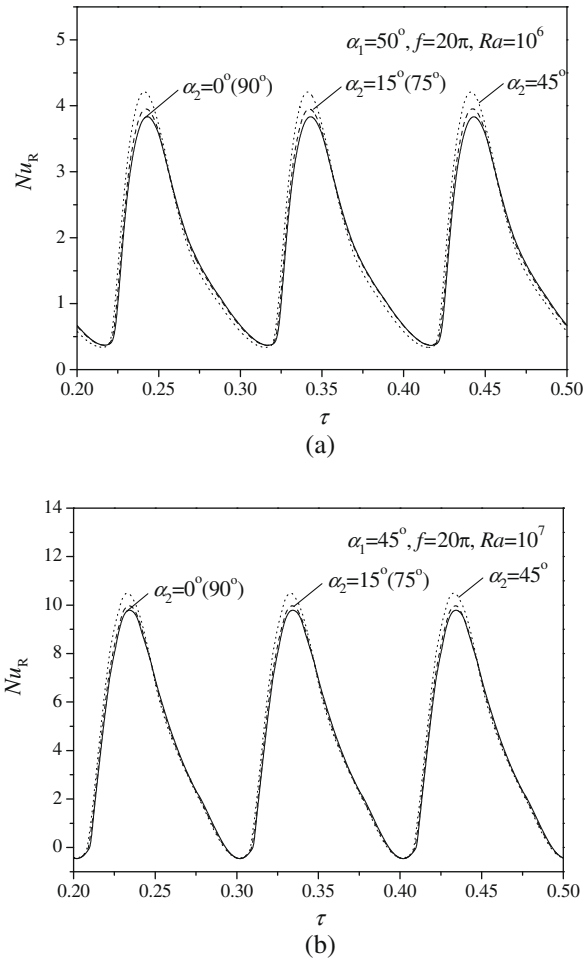


**Fig. 8.** Variations of the average Nusselt number on the right side wall with time for different $\alpha_2$ ($Da = 10^{-3}$, $Pr = 1.0$, $\varepsilon = 0.6$, $\sigma = 1.0$, $f = 20\pi$ and $\tau_p = 0.1$).

These findings indicate that, when the porous cavity is inclined with three-dimensional method, the flow patterns inside are more complicated and the heat transfer performance would be different.

The periodic oscillations of average Nusselt number on the right side wall ($Nu_R$, $X = 1$) with $Ra = 10^6$ and $Ra = 10^7$ are presented in Fig. 8. It is shown that, with different inclination angles, such as $\alpha_2 = 0°$, 15°, 45°, 75° and 90°, the Nusselt numbers oscillate with time smoothly and the time-averaged values are lager than zero.

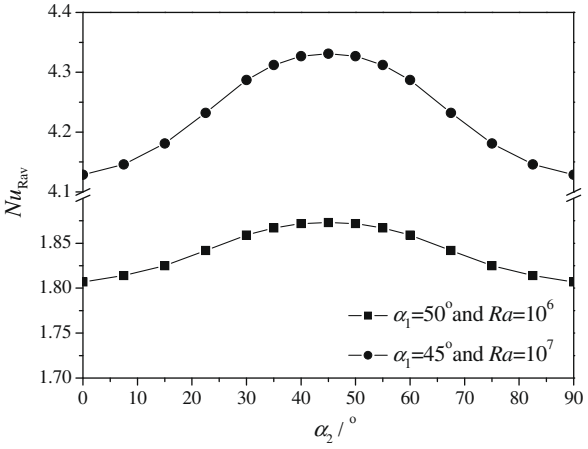


**Fig. 9.** Variations of the time-averaged Nusselt number on the right side wall with $\alpha_2$ ($Da = 10^{-3}$, $Pr = 1.0$, $\varepsilon = 0.6$, $\sigma = 1.0$, $f = 20\pi$ and $\tau_p = 0.1$).

It is obvious that, when $\alpha_2$ is equal to 45°, the heat transfer is better. The variations of time-averaged Nusselt number on the right side wall ($Nu_{Rav}$, $X = 1$) with $Ra = 10^6$ and $Ra = 10^7$ are presented in Fig. 9. It shows that, as $\alpha_2$ increases from 0° to 90°, the Nusselt number increases first and then decreases. The maximal heat fluxes are obtained at $\alpha_2 = 45°$. This suggests that, when $\alpha_1$ is fixed, the natural convection heat transfer in the porous cavity can be further improved with proper selection of $\alpha_2$. However, compared with the results demonstrated in Figs. 5 and 6, it is found that, the effect of $\alpha_2$ is relatively small and the natural convection in the porous cavity is mainly affected by $\alpha_1$. This is because, in the present study, the heating and cooling surfaces are perpendicular to $x$-axis and the flow patterns inside are mainly controlled by $\alpha_1$, which makes the effect of $\alpha_2$ relatively small.

### 4.3. Effect of temperature oscillation frequency

Finally, the effect of temperature oscillation frequency is carefully examined. In this case, the porous cavity is inclined around both $x$ and $y$ axes with the optimal inclination angles of $\alpha_1 = 50°$, $\alpha_2 = 45°$ with $Ra = 10^6$ and $\alpha_1 = 45°$, $\alpha_2 = 45°$ with $Ra = 10^7$, respectively, and the oscillation frequency $f$ changes from $5\pi$ to $90\pi$. The computations are performed with the other parameters kept constant: $Da = 10^{-3}$, $Pr = 1.0$, $\varepsilon = 0.6$, $\sigma = 1.0$.

The periodic oscillations of average Nusselt number on the right side wall ($Nu_R$, $X = 1$) with $Ra = 10^6$ and $Ra = 10^7$ are presented in Fig. 10. It is shown that, with different oscillation frequencies, such

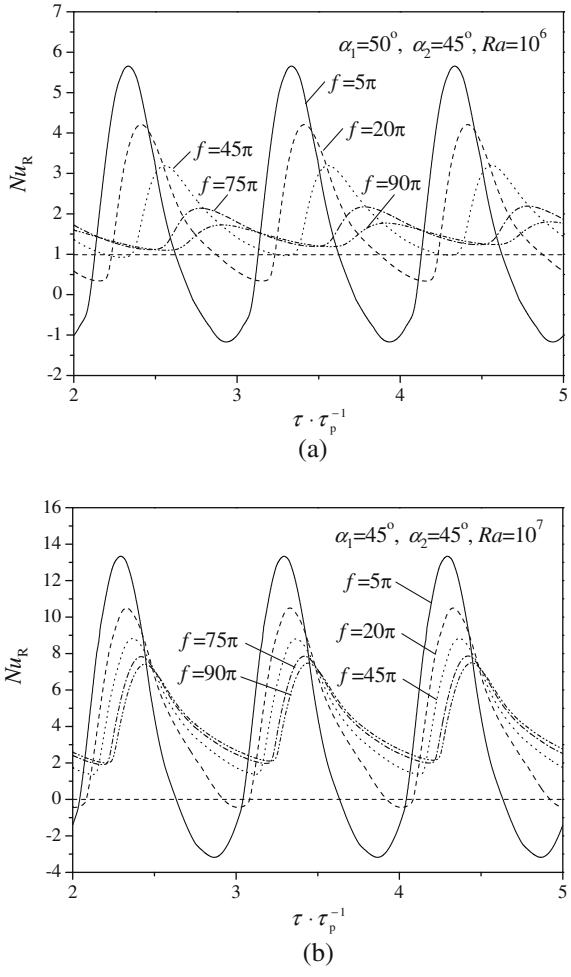


**Fig. 10.** Variations of the average Nusselt number on the right side wall with time for different temperature oscillation frequency ($Da = 10^{-3}$, $Pr = 1.0$, $\varepsilon = 0.6$ and $\sigma = 1.0$).

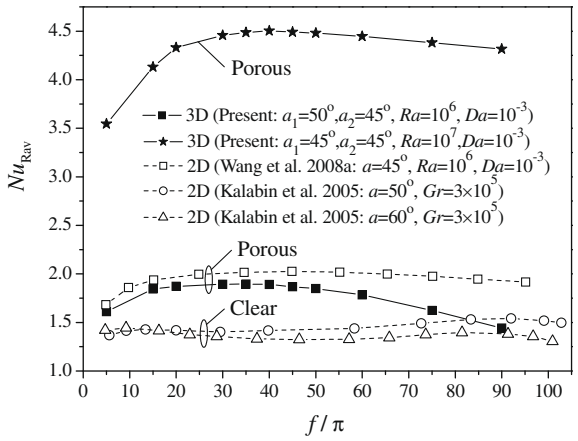


**Fig. 11.** Variations of the time-averaged Nusselt number on the right side wall with temperature oscillation frequency ($Da = 10^{-3}$, $Pr = 1.0$, $\varepsilon = 0.6$ and $\sigma = 1.0$).

as $f = 5\pi$, $20\pi$, $45\pi$, $70\pi$ and $90\pi$, the Nusselt numbers oscillate with time smoothly and the time-averaged values are lager than zero. It is obvious that, as the frequency increases, the amplitudes of the Nusselt numbers decrease. This is because, as the frequency increases, the temperature on the lower side wall ($X = 0$) oscillates more quickly and the flow patterns inside can not response and transit as rapidly as possible, which finally leads to the heat transfer delays and Nusselt number amplitude reductions. These findings also agree with the results obtained by Kalabin et al. (2005) and Wang et al. (2008a). The variations of the time-averaged Nusselt number on the right side wall ($Nu_{Rav}$, $X = 1$) with $Ra = 10^6$ and $Ra = 10^7$ are presented in Fig. 11. It is shown that, as the frequency increases from $5\pi$ to $90\pi$, the Nusselt number increases first and then decreases, the maximal heat fluxes are obtained at $f = 35\pi$ ($\alpha_1 = 50°$, $\alpha_2 = 45°$) as $Ra$ equals $10^6$ and $f = 40\pi$ ($\alpha_1 = 45°$, $\alpha_2 = 45°$) as $Ra$ equals $10^7$, respectively. Furthermore, when the frequency is in the range of $30\pi$–$50\pi$, the heat transfer performances are also satisfactory. This suggests that, with proper combinations of oscillating frequency and inclination angles, such as $f = 35\pi$, $\alpha_1 = 50°$ and $\alpha_2 = 45°$ with $Ra = 10^6$ and $f = 40\pi$, $\alpha_1 = 45°$ and $\alpha_2 = 45°$ with $Ra = 10^7$, the natural convection heat transfer in three-dimensional porous system will be significantly improved and optimized.

## 5. Conclusions

Three-dimensional natural convections in an inclined porous cavity with time oscillating boundary conditions are investigated in this paper. The combination effects of inclination angles ($\alpha_1$, $\alpha_2$) and temperature oscillation frequency ($f$) on the convection characteristics with different Rayleigh numbers ($Ra = 10^6$ and $10^7$) are carefully investigated, especially when the porous cavity is seriously inclined ($80° \leqslant \alpha_1 \leqslant 90°$), and some new transport phenomena are observed. The major findings are as follows:

Firstly, it is revealed that, when the porous cavity is moderately inclined ($0° \leqslant \alpha_1 \leqslant 75°, \alpha_2 = 0°$), the natural convections inside are stable, regular and quasi two-dimensional, which are similar to those of Wang et al. (2008a). However, if the cavity is more seriously inclined ($75° \leqslant \alpha_1 \leqslant 90°, \alpha_2 = 0°$), the flow patterns inside are unstable and much more complicated, and the three-dimensional multiple roll-cells with different intercrossing angles are established, which would finally lead to complicated heat transfer performances.

Secondly, it is found that, when the porous cavity is three-dimensionally inclined ($\alpha_1 > 0°$, $\alpha_2 > 0°$), the natural convections are quite different and a series of three-dimensional screw type flexural roll-cells are established. It is also shown that, when $\alpha_1$ is fixed, the natural convection heat transfer can be further improved by changing $\alpha_2$ and the optimal inclination status are obtained at $\alpha_1 = 50°$, $\alpha_2 = 45°$ as $Ra = 10^6$ and $\alpha_1 = 45°$, $\alpha_2 = 45°$ as $Ra = 10^7$, respectively. With these optimal inclination angles, the maximal heat fluxes in the porous cavity are finally obtained at the optimal frequencies of $f = 35\pi$ with $Ra = 10^6$ and $f = 40\pi$ with $Ra = 10^7$, respectively.

The above conclusions would be useful for further understanding and optimizing the natural convections in three-dimensional porous media systems.

## Acknowledgements

We would like to acknowledge financial supports for this work provided by the National Natural Science Foundation of China (No. 50806056) and National Defense Science and Technology Key Laboratory Foundation of China (No. 9140C7102010804).

## References

Antohe, B.V., Lage, J.L., 1994. A dynamic thermal insulator: inducing resonance within a fluid saturated porous medium enclosure heated periodically from the side. Int. J. Heat Mass Transfer 37 (5), 771–782.
Basak, T., Roy, S., Singh, S.K., Pop, I., 2009. Finite element simulation of natural convection within porous trapezoidal enclosures for various inclination angles: effect of various wall heating. Int. J. Heat Mass Transfer 52 (19–20), 4135–4150.
Ergun, S., 1952. Fluid flow through packed columns. Chem. Eng. Prog. 48 (2), 89–94.
Kalabin, E.V., Kanashina, M.V., Zubkov, P.T., 2005. Natural-convective heat transfer in a square cavity with time-varying side-wall temperature. Numer. Heat Transfer, Part A 47 (6), 621–631.
Kazmierczak, M., Chinoda, Z., 1992. Buoyancy-driven flow in an enclosure with time-periodic boundary condition. Int. J. Heat Mass Transfer 35 (6), 1507–1518.
Kladias, N., Prasad, V., 1991. Experimental verification of Darcy–Brinkman–Forchheimer flow model for natural convection in porous media. J. Thermophys Heat Transfer 5 (4), 560–576.
Kwak, H.S., Hyun, J.M., 1996. Natural convection in an enclosure having a vertical sidewall with time-varying temperature. J. Fluid Mech. 329, 65–88.
Kwak, H.S., Kuwahara, K., Hyun, J.M., 1998. Resonant enhancement of natural convection heat transfer in a square enclosure. Int. J. Heat Mass Transfer 41 (18), 2837–2846.
Lundgren, T.S., 1972. Slow flow through stationary random beds and suspensions of spheres. J. Fluid Mech. 51, 273–299.
Nield, D.A., Bejan, A., 2006. Convection in Porous Media, third ed. Springer, New York.
Nithyadevi, N., Kandaswamy, P., Sivasankaran, S., 2006. Natural convection in a square cavity with partially active vertical walls: time-periodic boundary condition. Math. Probl. Eng. 2006, 1–16.
Ozoe, H., Sayama, H., Churchill, S.W., 1974. Natural convection in an inclined square channel. Int. J. Heat Mass Transfer 17 (3), 401–406.
Ozoe, H., Yamamoto, K., Churchill, S.W., 1979. Three-dimensional numerical analysis of natural convection in an inched channel with a square cross section. AICHE J. 25 (4), 709–716.
Oztop, H.F., 2007. Natural convection in partially cooled and inclined porous rectangular enclosures. Int. J. Therm. Sci. 46 (2), 149–156.
Patankar, S.V., 1980. Numerical Heat Transfer and Fluid Flow. McGraw-Hill, New York.
Pop, I., Ingham, D.B., 2001. Convective Heat Transfer: Mathematical and Computational Modeling of Viscous Fluids and Porous Media. Pergamon, Oxford.
Reeve, H.M., Mescher, A.M., Emery, A.F., 2004. Unsteady natural convection of air in a tall axisymmetric, nonisothermal annulus. Numer. Heat Transfer, Part A 45 (7), 625–648.
Rudraiah, N., Malashetty, M.S., 1990. Effect of modulation on the onset of convection in sparsely packed porous layer. J. Heat Transfer 112 (3), 685–689.
Soong, C.Y., Tzeng, P.Y., Hsieh, C.D., 2001. Numerical study of bottom-wall temperature modulation effects on thermal instability and oscillatory cellular convection in a rectangular enclosure. Int. J. Heat Mass Transfer 44 (20), 3855–3868.
Vafai, K., 2005. Handbook of Porous Media, second ed. CRC Press, Boca Raton.
Varol, Y., Oztop, H.F., Pop, I., 2008. Numerical analysis of natural convection in an inclined trapezoidal enclosure filled with a porous medium. Int. J. Therm. Sci. 47 (10), 1316–1331.
Wang, Q.W., Wang, G., Zeng, M., Ozoe, H., 2008. Uni-directional heat flux through the horizontal fluid layer with sinusoidal wall temperature at the top or bottom boundaries. Int. J. Heat Mass Transfer 51 (7–8), 1675–1682.
Wang, G., Wang, Q.W., Zeng, M., Ozoe, H., 2008a. Numerical study of natural convection heat transfer in an inclined porous cavity with time-periodic boundary conditions. Transp. Porous Med. 74 (3), 293–309.

Wang, G., Wang, Q.W., Zeng, M., Ozoe, H., 2008b. Natural convection heat transfer in an inclined porous cavity under time-periodic boundary conditions with positive/negative inclined angles. J. Porous Media 11 (6), 541–555.

Xia, Q., Yang, K.T., Mukutmoni, D., 1995. Effect of imposed wall temperature oscillations on the stability of natural convection in a square enclosure. J. Heat Transfer 117 (1), 113–120.